2015

A class of rare antiferromagnetic metallic oxides: double perovskite AMn(3)V(4)O(12) (A = Na+, Ca2+, and La3+) and the site-selective doping effect

Guangbiao Zhang
Henan University

Yuan Xu Wang
Henan University

Zhenxiang Cheng
University of Wollongong, cheng@uow.edu.au

Yuli Yan
Henan University

Chengxiao Peng
Henan University

See next page for additional authors

Publication Details

Zhang, G., Wang, Y., Cheng, Z., Yan, Y., Peng, C., Wang, C. & Dong, S. (2015). A class of rare antiferromagnetic metallic oxides: double perovskite $AMn_3V_4O_{12}$ (A = Na^+, Ca^{2+}, and La^{3+}) and the site-selective doping effect. Physical Chemistry Chemical Physics, 17 (19), 12717-12721.

A class of rare antiferromagnetic metallic oxides: double perovskite AMn(3)V(4)O(12) (A = Na+, Ca2+, and La3+) and the site-selective doping effect

Abstract

We have investigated the structural, electronic, and magnetic properties of A-site-ordered double-perovskitestructured oxides, $AA'_3B_4O_{12}$ (A = Na, Ca, and La) with Mn and V at A' and B sites, respectively, using firstprinciple calculations based on the density functional theory. Our calculation results show that the antiferromagnetic phase is the ground state for all the compounds. By changing the A-site ions from Na^+ to Ca^{2+} and then to La^{3+}, the transfer of charge between Mn and O ions was changed from 1.56 to 1.55 and then to 1.50, and that between the V and O ions changed from 2.01 to 1.95 and then to 1.93, revealing the cause for the unusual site-selective doping effect. Mn 3d electrons dominate the magnetic moment and are localized, with an intense hybridization with O 2p orbitals, which indicates that the magnetic exchange interaction between Mn ions is mediated through O and that the super exchange mechanism will take effect. These materials have a large one-electron bandwidth W, and the ratio of the on-site Coulomb repulsion U to W is less than the critical value $(U/W)_c$, which leads to metallic behavior of $AMn_3V_4O_{12}$. This is further evidenced by the large number of free electrons contributed by V at the Fermi surface. These calculations, in combination with the reported experimental data, prove that these double perovskites belong to the rare antiferromagnetic metallic oxides.

Keywords

3, v, 4, o, 12, na, ca2, la3, site, selective, doping, rare, effect, antiferromagnetic, metallic, oxides, double, perovskite, amn, class

Disciplines

Engineering | Physical Sciences and Mathematics

Publication Details

Zhang, G., Wang, Y., Cheng, Z., Yan, Y., Peng, C., Wang, C. & Dong, S. (2015). A class of rare antiferromagnetic metallic oxides: double perovskite $AMn_3V_4O_{12}$ (A = Na^+, Ca^{2+}, and La^{3+}) and the site-selective doping effect. Physical Chemistry Chemical Physics, 17 (19), 12717-12721.

Authors

Guangbiao Zhang, Yuan Xu Wang, Zhenxiang Cheng, Yuli Yan, Chengxiao Peng, Chao Wang, and Shuai Dong

A class of rare antiferromagnetic metallic oxides: Double Perovskite $AMn_3V_4O_{12}$ (A = Na^+, Ca^{2+}, and La^{3+}) and Site-Selective Doping Effect

Guangbiao Zhang,[a] Yuanxu Wang,[*a] Zhenxiang Cheng,[*a,b] Yuli Yan,[a] Chengxiao Peng,[a] Chao Wang,[a] and Shuai Dong[c]

Received Xth XXXXXXXXXX 20XX, Accepted Xth XXXXXXXXX 20XX
First published on the web Xth XXXXXXXXXX 200X
DOI: 10.1039/b000000x

We have investigated the structural, electronic, and magnetic properties of A-site-ordered double perovskite-structured oxides $AA'_3B_4O_{12}$ (A = Na, Ca, and La) with Mn and V at A′ and B site, respectively, using the first-principle calculation based on the density functional theory. Our calculation results show that the antiferromagnetic (AFM) phase is the ground state for all the compounds. By changing the A-site ions from Na^+ to Ca^{2+} and then to La^{3+}, the transfer of charge of Mn ions changed from 1.56 to 1.55 and to 1.50 and ones of V ions changed from 2.01 to 1.95 and to 1.93, revealing the cause for the unusual site-selective doping effect. Mn 3d electrons dominate magnetic moment and localized, with an intense hybridization with O 2p orbital, which indicates that the magnetic exchange interaction between Mn atoms is mediated through O and super exchange mechanism will take effect. These materials have large one-electron bandwidth W, and the radio of the on-site Coulomb repulsion U to W is less than a critical value $(U/W)_c$, which leads to metallic behavior of $AMn_3V_4O_{12}$. This is further evidenced by the large number of free electrons contributed by V at the Fermi surface. This calculation work, in combination with the reported experimental data, proves that these studied double perovskites belong to the rare antiferromagnetic metallic oxides.

1 Introduction

The A-site-ordered double perovskites with the general chemical formula $AA'_3B_4O_{12}$ (sometimes B site can accommodate two different elements) have received extensive attention both in theory and experiment owning to their special ordered structures and wide variety of intriguing physical properties[1–5]. For instance, colossal magnetoresistance under weak magnetic fields, giant dielectric constant over a wide temperature range, and high temperature ferromagnetic transitions were found in such perovskites. Furthermore, the double perovskite structures provide an excellent playground to delicately tune their physical properties by accommodating substitution atoms at many sites, A, A′, and B. These compounds crystallize with a $Im\bar{3}$ cubic lattice in which the A- and A′-site cations are at the originally 12-fold-coordinated site in a simple ABO_3 perovskite. The BO octahedral in this structure is fairly rigid but heavily tilted. The B-O-B angle deviates significantly away from 180°, leading to the formation of square-planar coordinated $A'O_4$ units. The A′ sites are usually filled with transition-metal Jahn-Teller active ions Cu^{2+} and Mn^{3+}. For example, $ACuM_3Mn_4O_{12}$ (A = Ca, La, or Bi) were observed high-temperature ferromagnetic transitions due to the couplings between the spins at A′-site Cu and B-site Mn above room temperature[6–8]. $LaCu_3Fe_4O_{12}$ and $BiCu_3Fe_4O_{12}$ show intersite charge transfer between the A-site Cu and B-site Fe ions, leading to paramagnetism-to-antiferromagnetism and accompanied metal-to-insulator (semiconductor) isostructural phase transitions[9,10]. In $CaCu_3B_4O_{12}$ [11], the CuO_4 planes with Jahn-Teller Cu^{2+} ions align perpendicular to each other. This special alignment enable direct exchange interaction between the nearest Cu^{2+} spins, which gives rise to ferromagnetic behavior in $CaCu_3Ge_4O_{12}$ and $CaCu_3Sn_4O_{12}$. Whereas in $CaCu_3Ti_4O_{12}$, superexchange interaction exists due to the Cu(3d)-O(2p)-Ti(3d) orbital hybridization, resulting in an antiferromagnetic insulating state and making the observation of colossal dielectric constant observation possible. In $YMn_3Al_4O_{12}$ [4], the half-filled d_{r2-z2} and d_{xy} orbitals of the nearest neighboring Mn ions are directed toward each other. The overlap of those orbitals produces antiferromagnetic direct exchange interaction between the Mn spins. Therefore, it is quite obvious that charge transfer and orbit hybridization in $AA'_3B_4O_{12}$ compounds are critical for showing rich physics ranging from

0 [a]*Institute for Computational Materials Science, School of Physics and Electronics, Henan University, Kaifeng, 475004, People's Republic of China. E-mail: wangyx@henu.edu.cn*
0 [b]*Institute for Superconducting & Electronic Materials (ISEM), University of Wollongong, North Wollongong NSW 2500, Australia. E-mail: cheng@uow.edu.au*
0 [c]*Department of Physics, Southeast University, Nanjing, 211189, People's Republic of China*

metal/insulator, ferromagnetism(FM)/antiferromagnetism and colossal magnetic resistance effect, to giant dielectric constant. The understanding of the mechanism behind of these rich physics will help for the rational development of materials with superior properties.

Furthermore, antiferromagnetic metallic perovskite oxide is very rare. The transition-metal oxides belong to two categories, viz. the Mott-Hubbard type and the charge-transfer type[12]. The basis for such a classification depends on the relative value of the on-site Coulomb repulsion (U) between the d electrons and the one-electron bandwidth (W)[13]. In the limit of large U, a system is Mott-Hubbard insulator and the 3d orbit is single occupied sites. It can be described by the antiferromagntic Heisenberg spin model. On the other hand, in the opposite limit of large W, a system of uncorrelated half filled band becomes nonmagnetic metal. However, some perovskite transition-metal oxides have a strong hybridization between the metal 3d and O 2p orbits. It leads to an intermediate value of U/W. Examples include $CaCrO_3$[13], $(La_{1-z}Nd_z)_{1-x}Sr_xMnO_3$[14], $Pr_{0.5}Sr_{0.5}MnO_3$[15], etc., and such a system has an antiferromagnetic metal ground state. Although those materials are very useful for novel antiferromagnetic spintronic devices, they are very rare.

Very recently, a site ordered double perovskite $AMn_3V_4O_{12}$ (A = Na, Ca, La) were synthesized using high pressure-high temperature method by Zhang et al.[16] It has been shown experimentally that such a system has an antiferromagnetic/spin glass metallic ground state accompanying with metallic behavior. In this study, we proposed that such a perovskite structured system with two positions can be played with in its structure, in contrast to simple perovskite, as a platform for rare antiferromagnetic metallic oxides, and studied their mechanism using first-principle density function theory (DFT).

2 Computational Details

In this work, the structure optimization was carried out in the Kohn-Sham framework using the Vienna *ab initio* simulation package (VASP)[17–20], based on the projector augmented-wave method[21,22]. The exchange-correlation energy was treated in the local spin-density approximation (LSDA)[23]. The present calculations do not include spin-orbit corrections. The Na ($2p^63s^1$), Ca ($2p^63s^2$), La ($5s^25p^65d^16s^2$), Mn ($3p^63d^54s^2$), V ($3p^63d^44s^1$), and O ($2s^22p^4$) were treated as valence electrons. The plane wave cut-off energy was chosen to be 500 eV. The k-points of 7×7×7 were generated using the Monkhorst-Pack scheme[24] in the Brillouin zone. Brillion zone integrations were performed with a Gaussian broadening[25] of 0.2 eV during all relaxations. Structural optimizations with conjugate-gradient algorithm were continued until the Hellmann-Feynman forces on each ion to be less than 5 meV/Å. Experimentally established structural data[16] are used as input for the calculations.

In the LSDA+U framework[26,27], the strong Coulomb repulsion between localized d states is treated by adding a Hubbard-like term to the effective potential, leading to an improved description of correlation effects in transition-metal oxides. Since there is no unique way of including a Hubbard term within DFT framework, several different approaches exist, which all give similar results. To investigate the electron correlation effect on Mn and V 3d orbitals, we use the approach described by Dudarev et. al.[28] where only an effective Hubbard parameter $U_{eff} = U - J$ enters the Hamiltonian, where U and J are the Coulomb and exchange parameters, respectively. We applied the U_{Mn}=2, 4 eV and U_V= 2 eV. With these values of Hubbard parameter, caculated magnetic moment agree with experimental data[16].

3 Results and Discussion

The $AMn_3V_4O_{12}$ was a cubic A-site-ordered with a space group $Im\bar{3}$ (No. 204)[16], in which A, Mn, V, and O atoms were placed at the 2a (0, 0, 0), 6b (0, 1/2, 1/2), 8c (1/4, 1/4, 1/4), and 24g (x, y, 0) positions, respectively (shown as Figure 1 a). Experimentally established structure data were used as input for the calculations. The optimized structural parameters and selected bond lengths and angles of AMVO are listed in Table 1 along with experimental results for comparison. Both the theory and experiment results show that the lattice parameter, the Mn-Mn distance, the Mn-O distance, and the V-O distance will increase when the A-site ions change from Na to Ca and then to La due to the increased atomic size. The optimized structural parameters are less than the experimental ones. The underestimation of structural parameters for LDA comes from the overbind effect[29].

We calculated total energy with respect to the ground state magnetic configuration of $AMn_3V_4O_{12}$ using the LSDA method. To explore the structural phase stability of AMVO, we considered G-type antiferromagnetic (G-AFM), A-type antiferromagnetic (A-AFM), and ferromagnetic (FM) orderings. We found the G-AFM phase to be the ground state for NMVO. For $NaMn_3V_4O_{12}$ (NMVO), it is 47 meV/f.u. lower in energy than the A-AFM state and 35 meV/f.u. lower than FM state. For $CaMn_3V_4O_{12}$ (CMVO), it is 10 meV/f.u. lower than the A-AFM state and 19 meV/f.u. lower than FM state. For $LaMn_3V_4O_{12}$ (LMVO), it is 20 meV/f.u. lower than A-AFM state and 66 meV/f.u. lower than FM state.

Considering the electron correlation in the 3d transition-metal Mn and V ions, we calculated the electronic and magnetic properties of AMVO using the LSDA and LSDA+U method. The effective Hubbard parameter of Mn is 0 (LSDA), 2, and 4 eV and the ones of V is 0 (LSDA) and 2 eV. Figure 2 represents the total and site-decomposed density of states (DOS) in AFM configuration for AMVO. In agreement with the experimental results, it was found that the three compounds are metallic ev-

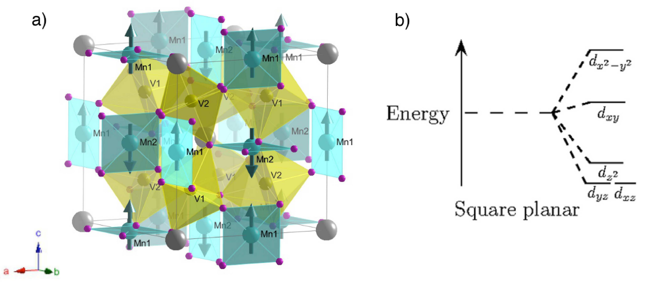

Fig. 1 a) Crystal structure of A-site-ordered pervoskite $AMn_3V_4O_{12}$ with $Im\bar{3}$. The arrow indicates the spin direct. b) Mn atom 3d sub-orbit diagram in compounds.

Table 1 Structural parameters and selected bond lengths and angles of NMVO, CMVO, and LMVO optimized by VASP, including the experimental (Exp.) structural parameters [16] as a reference.

	NMVO		CMVO		LMVO	
	Theo.	Exp.	Theo.	Exp.	Theo.	Exp.
a(Å)	7.2072	7.35514	7.2363	7.40704	7.30489	7.48485
O_x	0.3074	0.3023	0.3038	0.2944	0.3047	0.2947
O_y	0.1856	0.1917	0.1833	0.1936	0.1829	0.1957
Mn-O(Å)	1.928×4	2.032×4	1.943×4	2.092×4	1.955×4	2.124×4
	2.658×4	2.695×4	2.696×4	2.733×4	2.721×4	2.753×4
	3.169×4	3.169×4	3.176×4	3.147×4	3.213×4	3.170×4
V-O(Å)	1.906×6	1.925×6	1.908×6	1.927×6	1.926×6	1.944×6
V-O-V(deg)	141.9	145.6	142.2	147.98	141.8	148.6
Mn-O-Mn(deg)	102.4	101.4	101.3	99.4	101.5	99.6

idenced by large number of states around the Fermi surface. Therefore these compounds belong to a very rare class of materials, metallic antiferromagnetic perovskite oxides. Although the bands at Fermi surface are mainly composed of bands from V, a very small portion of contribution from O and Mn are also observed, which indicates a certain degree of orbit of hybridization among orbits of these ions. For NMVO, the bands (at about -2 eV), which are composed of Mn 3d and O 2p orbitals, suggest the Mn-O considerable covalent hybridization, which indicates a superexchange mechanism for the antiferromagnetism. However, Mn-O squares do not share oxygen, instead, they form O-Mn-O-O-Mn paths. The Mn-O-Mn superexchange interaction do not seem to be responsible for the antiferromagnetism of AMVO because one of the Mn-O bond lengths (greater than 2.6 Å) in the Mn-O-Mn paths is too long to mediate such interaction and because the Mn-O-Mn bond angle (about 103°) is far from the 180° expected to induce antiferromagnetic interaction according to the Kanamori-Goodenough rule [30–32]. The orbit hybridization of V, O, and Mn orbit at the Fermi surface indicates that B-site V ions may mediate the antiferromagnetic interaction between the Mn spins through Mn-O-V-O-Mn paths. This may be the origin of antiferromagnetism

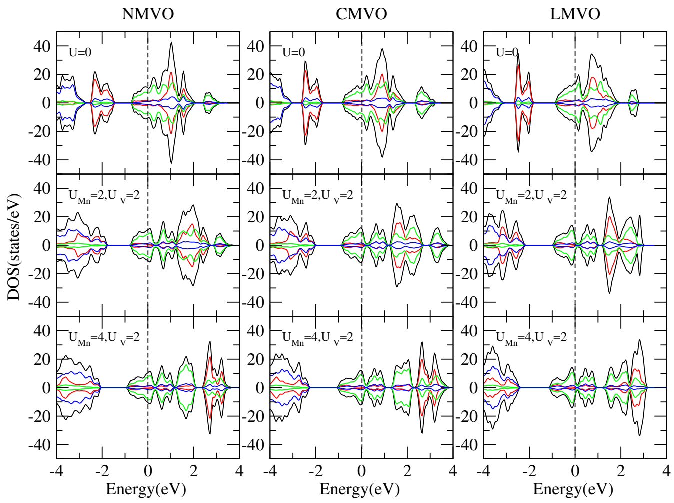

Fig. 2 The total and site-decomposed electronic DOS for AFM configuration of NMVO, CMVO, and LMVO obtained by LSDA and LDA+U calculation: total DOS (black), Mn (red), V (green), O (blue). The vertical dot-dash line at zero indicates the Fermi energy level.

in such metallic systems [4].

The LSDA+U results still keep their metallic character. The band gap between conductantion bands and valance bands enlarged due to orbital shifting towards higher energy with the increasing of U value. The band gap increases from 0.8 to 1.1 and then to 1.2 eV with U_{Mn} increasing from 0 to 4 eV and U_V increasing from 0 to 2 eV. Meanwhile, the calculated magnetic moment at the Mn-site changes from 3.70 to 4.14 μ_B, from 3.75 to 4.21 μ_B, and from 3.76 to 4.24 μ_B with U_{Mn} increasing from 0 to 4 eV for NMVO, CMVO, and LMVO, respectively. However, the calculated magnetic moment at the V-site changes from 0.01 to 0.99 μ_B, from 0.35 to 1.20 μ_B, and from 0.78 to 1.41 μ_B with U_V increasing from 0 to 2 eV for NMVO, CMVO, and LMVO, respectively. The qualitative change indicated that the electronic repulsion of V 3d electron is much correlated within AMVO.

The partial density of states (PDOS) of Mn1 in three compounds, NMVO, CMVO, and LMVO are shown in Figure 3, respectively. The doped electrons of the A′-site Mn ions are mainly localized below the Fermi surface, in addition to a very small portion of electrons at the Fermi surface, which means that Mn ions are responsible for the magnetic moment in the compounds. While the electrons of B-site V ions are mainly located at the Femi surface, which means that they are delocalized and contribute to the conductivity. According to the PDOS, energy level diagrams of A′-site Mn 3d orbits in the three compounds are plotted, shown as Figure 1b. Mn $3d_{yz}$, $3d_{xz}$, $3d_{x^2}$, $3d_{y^2}$ sub-orbits are occupied with electrons and located around 2 eV below the Fermi level, while $3d_{xy}$ located

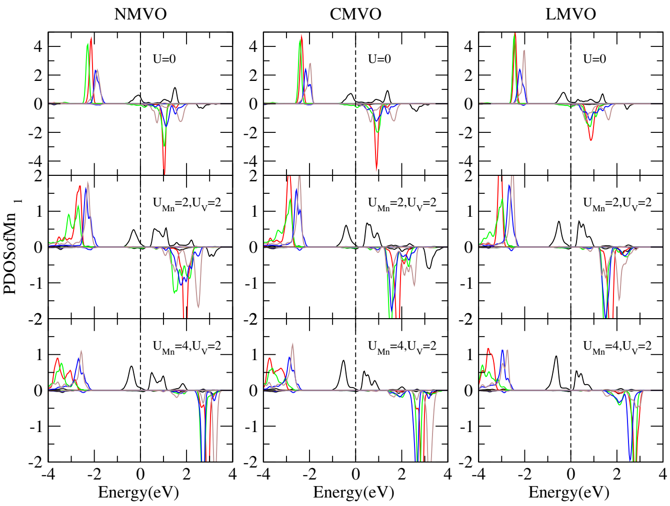

Fig. 3 The PDOS of Mn for AFM configuration of a) NMVO, b) CMVO, and c) LMVO obtained by LDA and LDA+U calculation: d_{xy} (black), d_{yz} (red), d_{xz} (green), d_{z^2} (blue), d_x^2 (brown). The vertical dot-dash line at zero indicates the Fermi energy level.

at the Fermi surface with partial occupation of electrons. This indicates that Mn $3d_{xy}$ electrons partially contribute to the conductivity of the compounds in addition to the contribution to the magnetic moment. It indicates that the Mn is at high spin states in all the three compounds. The calculated magnetic moment are smaller than the expected magnetic moment value of 5 μ_B [33]. Due to the partially occupation of $3d_{xy}$ orbit and the Mn-O considerable covalent hybridization, a small magnetic moment presents at the oxygen sites. These values are 0.04, 0.04, and 0.03 for NMVO, CMVO, and LMVO, respectively. This further proves that the Mn 3d, O 2p, V 3d O orbit hybridization is the key to the antiferromagnetic ordering in these compounds.

The V-O distances are 1.906, 1.908, 1.926 Åfor NMVO, CMVO, and LMVO, respectively. These values are similar to the average values of V-O distance of metallic perovskite-type V oxides for $SrVO_3$ (1.921 Å)[34], $MnVO_3$ (1.938 Å)[33], and $CaVO_3$ (1.963 Å)[35] and less than the average values of V-O distance of insulated perovskite-type V oxides for $ScVO_3$ (2.003Å)[36], YVO_3 (2.007 Å)[37], and $LaVO_3$ (2.042 Å)[37]. The short V-O distance means the strong hybridization of V 3d and O 2p orbitals, and it leads to a large one-electron bandwidth W. In the intermediate value of U/W, the materials are metal.

We also use Bader's "Atoms in molecules" theory[38,39] to analyze the valence states of Mn and V ions. Our calculation found that the transfer of charge of Mn ions changed from 1.56 to 1.55 and 1.50, and ones of V ions changed from 2.01 to 1.95 and to 1.93 by changing the A-site ions from Na^+ to Ca^{2+} and to La^{3+}. These results are consistent with the observed results of the difference charge density, supporting the site-selective doing effect in these compounds.

4 Conclusions

In summary, based on the first-principle calculations, we have studied the structural, electronic, and magnetic properties of A-site-ordered perovskite-structure oxides with Mn and V at A and B sites, respectively. Total energy calculations reveal that the AFM phase has a lower energy than the FM phase. By changing the A-site ions from Na to Ca and from Ca to La, the transfer of charge of Mn ions changed from 1.56 to 1.55 and to 1.50, and ones of V ions changed from 2.01 to 1.95 and to 1.93. The hybridization of the A-site Mn 3d and O 2p orbital below Fermi surface dominates the magnetic moment. The values of V-O distances are similar to the average values of V-O distance of metallic perovskite-type V oxides. The short V-O distance means the large one-electron bandwidth W. When the radio U/W less than a critical value $(U/W)_c$, the materials are metallic. The mechanism for such unique metallic antiferromagnetic double perovskites oxide, Mn contribute magnetic moment while V contribute metallic, is different from the previous reported compound, like $CaCrO_3$, where Cr contributes both magnetic moment and free electron at the Fermi level. This understanding opens a new route to rational design of antiferromagnetic metallic oxides which will have application in novel spintronics devices. In addition, the flexible structure with modifiable both A(A′) and B site provides an excellent playground to play with by accommodating variable elements.

5 Acknowledgment

This research was sponsored by the National Natural Science Foundation of China (No. 21071045, U1204112, and 11305046), the Program for New Century Excellent Talents in University (No. NCET-10-0132), and Foundation of He'nan Educational Committee (No. 14B140003, 13A140076, 14A430029, and 14A140016). Z. X. Cheng thanks ARC for support through a Future Fellowship.

References

1 M. Imada, A. Fujimori and Y. Tokura, *Rev. Mod. Phys.*, 1998, **70**, 1039–1263.

2 E. Dagotto, T. Hotta and A. Moreo, *Physics Reports*, 2001, **344**, 1–153.

3 Y. Long, T. Saito, M. Mizumaki, A. Agui and Y. Shimakawa, *J. Am. Chem. Soc.*, 2009, **131**, 16244–16247.

4 T. Tohyama, T. Saito, M. Mizumaki, A. Agui and Y. Shimakawa, *Inorg. Chem.*, 2010, **49**, 2492–2495.

5 H. Li, S. Lv, Y. Bai, Y. Xia, X. Liu and J. Meng, *J. Comput. Chem.*, 2012, **33**, 82–87.

6 Z. Zeng, M. Greenblatt, M. A. Subramanian and M. Croft, *Phys. Rev. Lett.*, 1999, **82**, 3164–3167.

7 J. A. Alonso, J. Sánchez-Benítez, A. D. Andrés, M. J. Martínez-Lope, M. T. Casais and J. L. Martínez, *Applied Physics Letters*, 2003, **83**, 2623–2625.

8 K. Takata, I. Yamada, M. Azuma, M. Takano and Y. Shimakawa, *Phys. Rev. B*, 2007, **76**, 024429–.

9 Y. W. Long, N. Hayashi, T. Saito, M. Azuma, S. Muranaka and Y. Shimakawa, *Nature*, 2009, **458**, 60–U3.

10 Y. Long, T. Saito, T. Tohyama, K. Oka, M. Azuma and Y. Shimakawa, *Inorganic Chemistry*, 2009, **48**, 8489–8492.

11 H. Shiraki, T. Saito, T. Yamada, M. Tsujimoto, M. Azuma, H. Kurata, S. Isoda, M. Takano and Y. Shimakawa, *Phys. Rev. B*, 2007, **76**, 140403.

12 J. Zaanen, G. A. Sawatzky and J. W. Allen, *Phys. Rev. Lett.*, 1985, **55**, 418–421.

13 P. A. Bhobe, A. Chainani, M. Taguchi, R. Eguchi, M. Matsunami, T. Ohtsuki, K. Ishizaka, M. Okawa, M. Oura, Y. Senba, H. Ohashi, M. Isobe, Y. Ueda and S. Shin, *Phys. Rev. B*, 2011, **83**, 165132.

14 T. Akimoto, Y. Maruyama, Y. Moritomo, A. Nakamura, K. Hirota, K. Ohoyama and M. Ohashi, *Phys. Rev. B*, 1998, **57**, R5594–R5597.

15 R. Kajimoto, H. Yoshizawa, Y. Tomioka and Y. Tokura, *Phys. Rev. B*, 2002, **66**, 180402.

16 S. Zhang, T. Saito, M. Mizumaki, W.-t. Chen, T. Tohyama and Y. Shimakawa, *J. Am. Chem. Soc.*, 2013, **135**, 6056–6060.

17 G. Kresse and J. Hafner, *Phys. Rev. B*, 1993, **47**, 558–561.

18 G. Kresse and J. Hafner, *Phys. Rev. B*, 1994, **49**, 14251–14269.

19 G. Kresse and J. Furthmüller, *Computational Materials Science*, 1996, **6**, 15–50.

20 G. Kresse and D. Joubert, *Phys. Rev. B*, 1999, **59**, 1758–1775.

21 P. E. Blöchl, *Phys. Rev. B*, 1994, **50**, 17953–17979.

22 G. Kresse and D. Joubert, *Phys. Rev. B*, 1999, **59**, 1758–1775.

23 R. O. Jones and O. Gunnarsson, *Rev. Mod. Phys.*, 1989, **61**, 689–746.

24 H. Monkhorst and J. Pack, *Phys. Rev. B*, 1976, **13**, 5188–5192.

25 C. Elsässer, M. Fähnle, C. Chan and K. Ho, *Phys. Rev. B*, 1994, **49**, 13975–13978.

26 I. V. Solovyev, P. H. Dederichs and V. I. Anisimov, *Phys. Rev. B*, 1994, **50**, 16861–16871.

27 V. I. Anisimov, J. Zaanen and O. K. Andersen, *Phys. Rev. B*, 1991, **44**, 943–954.

28 S. Dudarev, G. Botton, S. Savrasov, C. Humphreys and A. Sutton, *Phys. Rev. B*, 1998, **57**, 1505–1509.

29 A. van de Walle and G. Ceder, *Phys. Rev. B*, 1999, **59**, 14992–15001.

30 J. B. Goodenough, *Phys. Rev.*, 1955, **100**, 564–573.

31 J. B. Goodenough, *Journal of Physics and Chemistry of Solids*, 1958, **6**, 287 – 297.

32 J. Kanamori, *Journal of Physics and Chemistry of Solids*, 1959, **10**, 87 – 98.

33 M. Markkula, A. M. Arevalo-Lopez, A. Kusmartseva, J. A. Rodgers, C. Ritter, H. Wu and J. P. Attfield, *Phys. Rev. B*, 2011, **84**, 094450.

34 Y. Lan, X. Chen and M. He, *Journal of Alloys and Compounds*, 2003, **354**, 95 – 98.

35 B. Chamberland and P. Danielson, *Journal of Solid State Chemistry*, 1971, **3**, 243 – 247.

36 G. Wang, J. Yang, C. Liu and M. Zhang, *Solid State Communications*, 2012, **152**, 2049–2052.

37 H. Sawada, N. Hamada, K. Terakura and T. Asada, *Phys. Rev. B*, 1996, **53**, 12742–12749.

38 R. F. W. Bader, in *Atoms in Molecules*, John Wiley & Sons, Ltd, 2002.

39 W. Tang, E. Sanville and G. Henkelman, *Journal of Physics-condensed Matter*, 2009, **21**, 084204.